

Experimental investigation on the near flow field of dual stream nozzles

S Sudhakar, N Karthikeyan and S Ashwin Kumar

Experimental Aerodynamics Division, CSIR-National Aerospace Laboratories,
Bangalore, India

E-mail: ssudha@nal.res.in

Abstract. An experimental investigation was carried out to investigate the effect of beveling of primary nozzle exit in the near field of a dual stream nozzle flow. Two exit geometry configurations of primary stream nozzle viz., (a) circular (b) bevel along with one exit geometry of the secondary stream-circular, were studied. Experiments were carried out at both subsonic and supersonic primary nozzle operating conditions $M_p=0.96$ and 1.2 . The secondary nozzle exit Mach number was maintained at 0.65 and 0.85 respectively to maintain the velocity ratio of 0.7 between the primary and secondary jet. The by-pass ratio for this investigation is maintained at 2.0 . Flow visualization using retro-reflective shadowgraph technique was used for the qualitative visualization of the near flow field at the Mach number of 1.2 . The mean and turbulent quantities in near flow field were obtained using particle image Velocimetry (2D-PIV). The flow visualization and PIV investigations show significant change in mean and turbulent quantities brought about in the near field due to the beveling of the primary nozzle. PIV results show increase in the potential core length and reduction in turbulence levels in the potential core by the secondary flow regardless of the jet exit geometry. A differential trend is seen in the shear layer growth and the turbulence characteristics between the shorter and longer lips sides of the beveled nozzle. In the dual stream configurations, bevel nozzle shows lower Reynolds stress values than the circular one except in the shorter lip side at the larger downstream locations.

1. Introduction

Jet noise continues to be an significant component of aircraft noise. Several research and development efforts are underway around the globe to completely understand the physics behind generation of jet noise and develop a suitable technique to reduce it. Efforts towards passive methods of jet noise suppression – especially for civil aircraft using turbo-fan engines- have progressed in tandem with the efforts towards understanding noise generation [1]. In the past, numerous concepts such as the incorporation of vortex generators, tabs, chevrons and other mixing devices, offset and non-concentric nozzles, thermal shielding, etc., have been investigated. However, none of these devices has produced the level of noise reduction necessary to provide a substantial and noticeable relief for the communities living around airports. In addition, most of such techniques have resulted in thrust, weight and drag penalties. Recently, studies carried out by Viswanathan [2-5] have shown that beveling of primary jet nozzle exit has resulted in reduced noise levels both in single and dual stream configurations. This approach has proven to be the most effective technique for jet noise suppression, particularly with simulated flight conditions. The beveled nozzle concept has lesser thrust penalties without no additional weight or drag. Further, the extension of the concept to a working model in existing engines is much easier.



Computational simulation studies, using LES/DES, carried out by Viswanathan et al [6-7] on dual stream with beveled primary nozzle to relate the flow field changes to the acoustic characteristics. However, there has been no attempt to validate the result of these studies against any standard experimental database. An understanding of the physical mechanisms that may be responsible for the observed noise reduction can only be arrived, through detailed experimental flow-field investigations. The present study attempts to simulate exit flow conditions of commercial high by-pass ratio turbofan jet engines (velocity ratio and Mach number of core flow) using cold jets to investigate the effect of primary nozzle exit beveling on the flow fields of a dual stream nozzle. 2D-particle image Velocimetry and retro-reflective shadowgraph techniques are used to relate the subtle changes in the flow field (caused due to primary jet exit beveling) for better insight and understanding of noise generation in dual stream nozzles flow.

2. Experimental setup

2.1. Test Facility

The measurements are carried out in the jet aeroacoustics research facility at EAD, CSIR-NAL (Figure 1). The jet is supplied with dry compressed air from a 10 bar reservoir through a computerized globe valve (Make: Fisher, Type: ET) with a Whisper Cage Trim for cutting down valve pins. The settling chamber is provided with a perforated cone and three sets of screens for flow conditioning. An inline electric heater, provided in-between the valve and the settling chamber allows for studies on hot

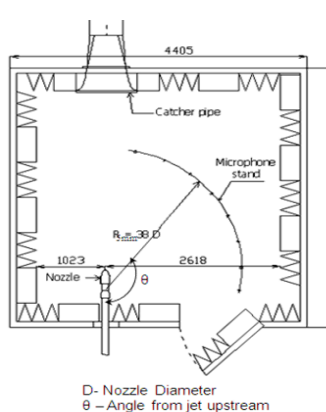


Figure 1. Schematic of jet acoustic research facility



2a) Circular primary nozzle



2b) Bevel primary nozzle



2c) Secondary Circular nozzle



Figure 3. Dual stream nozzle assembly

supersonic jets. The jet can be run continuously for up to 40 minutes. The driving pressure for the jet was maintained to within ± 0.35 psi of set pressure during the run. The jet exhausts in to an anechoic chamber of inner dimensions 3.6m (L) x 3.6m (W) x 3m (H) for carrying out acoustic measurements. The anechoic chamber walls are mounted with fiberglass covered acoustic wedges, which are designed to achieve a low-frequency cutoff of 300 Hz. The chamber is provided with suitable acoustically treated intakes to allow for entrainment by the jet. During the run, the ambient pressure in the chamber dropped by less than 0.1psi demonstrating that adequate area has been provided for entrainment. A catcher of 0.6m x 0.6m outlet provided with proper acoustic termination collects the jet exhaust. Preliminary acoustic tests showed that the room is anechoic above 400Hz with a partial floor grating in place.

2.2. Nozzle configuration

Figure 2. Shows the nozzle configuration used for the present study. Two primary nozzles (one with circular and one with 24° bevel) of different exit geometry and one secondary nozzle with circular exit has been fabricated to study the effect of primary nozzle exit beveling on flow field of the dual stream nozzle flow. The primary nozzle extends beyond the secondary nozzle exit to simulate actual engine nozzle configuration. The exit diameter of the primary nozzle is 38.1mm. The secondary nozzle has exit diameter 90.58mm. The exit bevel angle for the modified primary nozzle is 24°. The increase in exit area of the beveled nozzles is 3%. Photograph of dual stream nozzle flow arrangement through

combination of secondary and primary nozzle is shown in Figure 3. The exit area ratio between the secondary and the primary nozzle is 3.0.

Experiments planned on the selected nozzle configurations with different flow conditions are given in the following Table.1. The exit Mach number and velocity ratio for the present investigation is close to the jet Mach number of the aircraft during takeoff ($M_P=0.96$), climb and cruise ($M_P=1.2$) [1].

Table 1. Nozzle exit Mach numbers.

| | Primary(M_P) | Secondary(M_S) |
|--|------------------|--------------------|
| Circular primary nozzle | 0.96 | - |
| Circular primary nozzle | 1.2 | - |
| Beveled primary nozzle | 0.96 | - |
| Beveled primary nozzle | 1.2 | - |
| Dual stream with circular primary nozzle | 0.96 | 0.65 |
| Dual stream with circular primary nozzle | 1.2 | 0.85 |
| Dual stream with beveled primary nozzle | 0.96 | 0.65 |
| Dual stream with beveled primary nozzle | 1.2 | 0.85 |

2.3. Shadowgraph Set up

A retro-reflective type shadowgraph was setup (Figure 4) inside the anechoic chamber to capture the flow field of dual stream nozzle configurations. The set-up was that of a coincident double pass shadowgraph as described in [8]. Light from high power LED illuminator was converged on to the mirrored surface of a rod mirror fitted on to a glass filter just ahead of an IDT Y5[®] Camera. The reflected light from the rod mirror illuminated a region large enough to capture the jet from the nozzle exit. The illuminator provided a short light pulse of high energy of sufficient enough to uniformly illuminate the designated area for $5\mu s$ and was synchronized with the exposure of the camera fitted with a Nikkor 70-210 mm lens.

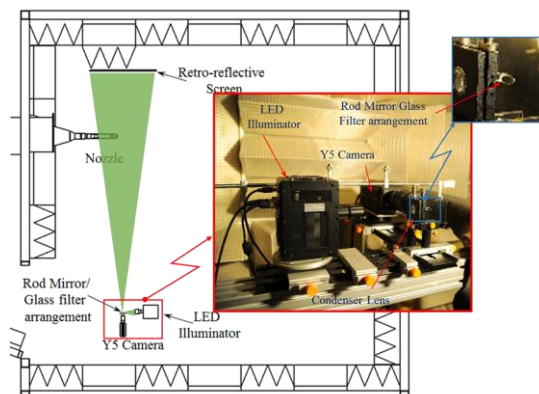


Figure 4. Shadowgraph setup

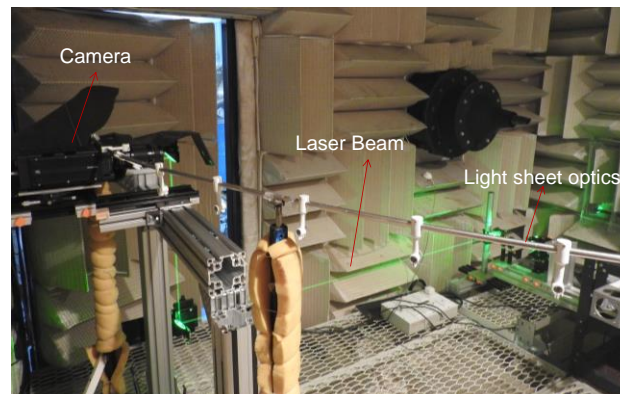


Figure 5. PIV setup

2.4. Particle Image Velocimetry

Figure 5 shows the setup for the 2-D PIV measurements inside the anechoic chamber of the jet acoustic research facility. The flow-field with tracer particles was illuminated by a double pulsed, frequency doubled dual Nd:YAG, PIV 400 laser, providing with a nominal 400 mJ of energy per pulse at a 532-nm wavelength. The optimum performance of the laser is at 15Hz (15 pairs per second). The light sheet optics are mounted to create sheet (380mmx300mm) in the streamwise plane at the center of the nozzle

cross section. The camera was mounted such that the light sheet and the camera image plane are parallel to acquire the image. The images are acquired using MotionPro® Y5 camera of 2314(H)X1728(V) pixels, with Nikkor® 75-210mm lens. The synchronization of laser and the camera image acquisition was achieved through IDT Motion-Pro® timing hub. The post processing of the acquired images were carried out with IDT ProVISION® XS software. Mean velocities were estimated from ensemble average of 2000 image pairs. The laser pulse separation time was kept at $3\mu\text{s}$ to allow the particle to move at least two pixels for the maximum velocity in the measurement. The velocity vectors were obtained from processing image with 48×48 pixel interrogation window with 50% overlap. A spatial resolution of 7.8mm in both directions(X and Y) was achieved. The flow field was seeded by injecting the fog of particle size $1\mu\text{m}$ in the settling chamber. The orientation of the nozzle for the PIV studies was such that shorter lip faced the floor of the anechoic chamber. As the light sheet for illumination was arranged from floor side of the chamber, this orientation prevents the obstruction of the illumination by the longer lip.

3. Results and Discussion

3.1. Shadowgraph

Figure 6a-d shows the flow field of the jet from circular and bevel nozzle with and without the presence of secondary stream captured using shadowgraph technique. Flow field for the primary jet from the circular nozzle at Mach number 1.2 is shown in figure 6a. The under expanded flow at the exit of the nozzle expands to adjust to the ambient. This is observed as a bulging jet at the primary nozzle exit. The ensuing flow features of shock cells are clearly captured in the shadowgraph. Three shock cells are

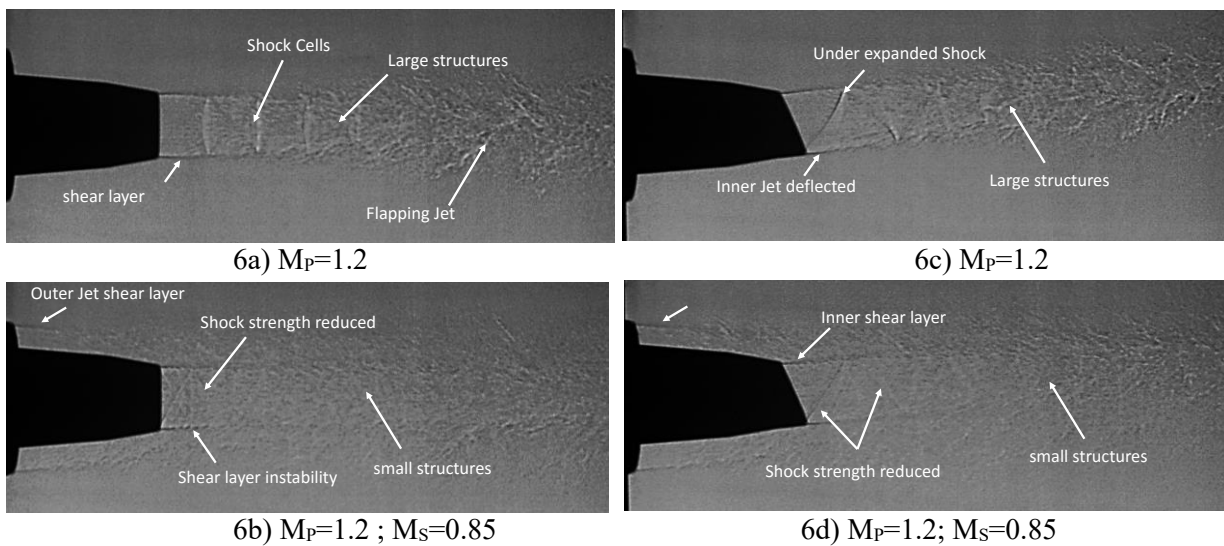


Figure 6. Shadowgraph images of the single and dual stream nozzle flow

discernable along with the shear layer emanating from the nozzle lip. Downstream of the third shock cell the jet dissipates into a flapping jet, the movement of which is captured in other shadowgraph realizations of the flow. In contrast the flapping of the jet is subdued when the secondary stream ($M_S=0.85$), is turned on as shown in figure 6b. Also introduction of secondary stream shows that the strength of the shock structures seen in the flow field of primary jet alone is heavily diminished. This is expected as the inner flow now exhausts into a different ambient dictated by the flow from the secondary stream. Since the under expanded jet from the inner nozzle cannot expand adequately at the exit due to the presence of secondary stream, it is deflected into itself resulting in oblique shocks at the exit of the primary jet. However these shocks are not as strong as the primary jet alone case and immediately dissipate, without forming any appreciable shock cells. Shear layers from the primary and secondary jets are captured clearly in the shadowgraph.

The shadowgraph of the flow field of the primary jet ($M_P=1.2$) from the beveled nozzle is shown in Figure 6c. Due to the extension of the lip on one side of the beveled nozzle, there is an azimuthal variation of the shear layer development, causing the flow to get inclined towards the shorter lip. The

initial flow from the nozzle exit shows that a shock emanating from the longer lip and interacting with the shear developing from the shorter lip. The shock reflects from the opposite shear layer tilting away from the edge. The flapping of the jet was not observed in beveled nozzle case. The number of shock cells seen is also lesser than that seen in the jet from the circular nozzle. When the secondary stream is turned on ($M_s=0.85$) the strength of the shock at the beveled nozzle exit is reduced (Figure 6d). The flow inclination angle is found to be decreased by the presence of the secondary stream. Hence the overall flow inclination angle is limited thus reducing even the minor thrust loss due to beveling of the primary inner nozzle. It is observed that the size of the turbulent flow structures seen in the primary jet alone case was reduced in the presence of secondary stream for both the circular and bevel nozzle cases.

3.2. Particle image velocimetry

Comparison of mean streamwise velocity field of the jet from circular and beveled nozzle with and without the presence of secondary stream at subsonic and supersonic exit Mach numbers of the primary jet, is shown in figure 7a-h. The width of the jet potential core for the primary jet alone at exit condition of $M_p=0.96$ (figure 7a) for the circular nozzle is higher than that seen for jet from the beveled nozzle

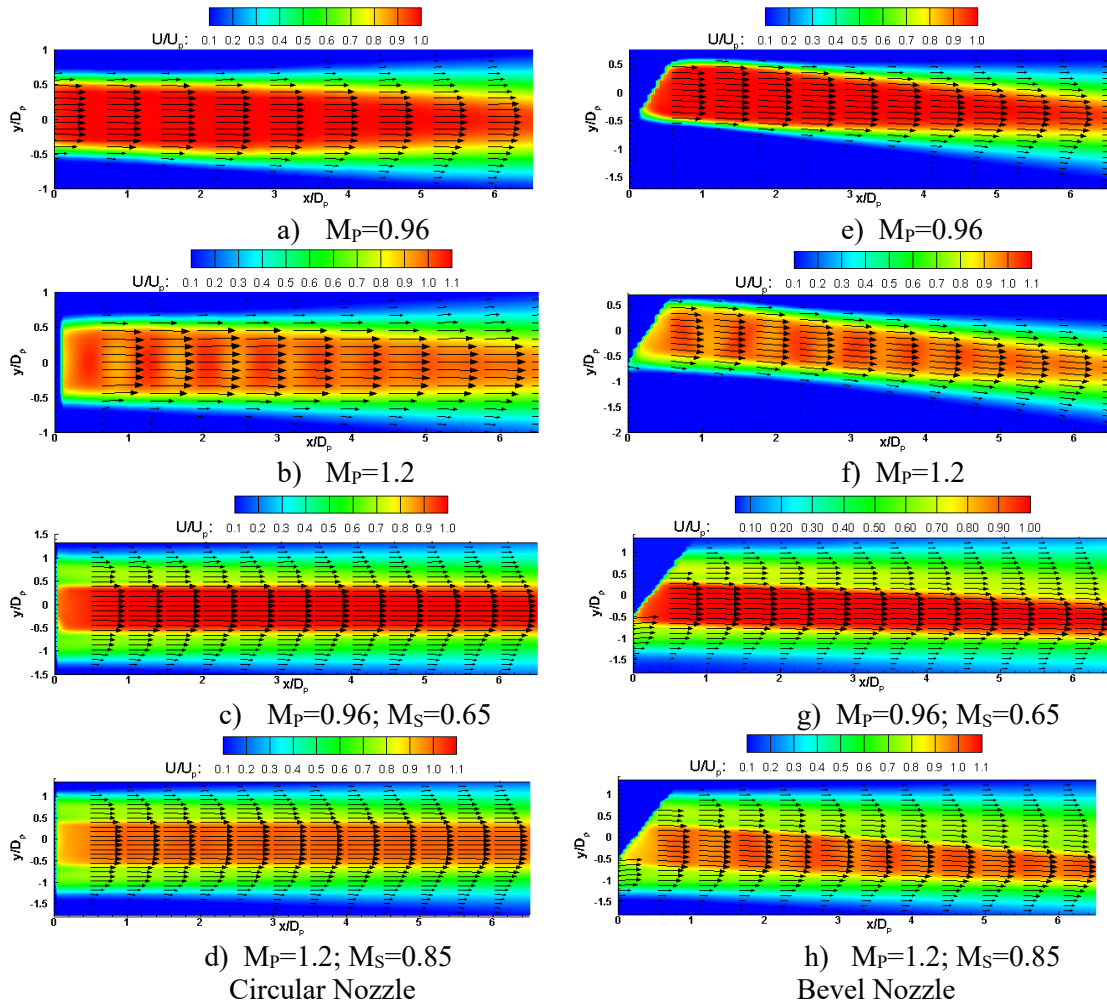


Figure 7. Mean streamwise velocity contour of single and dual stream nozzle flow

case (figure 7e). The jet flow field from the beveled nozzle is inclined towards the shorter lip of the nozzle at both subsonic and supersonic Mach number as seen in the shadowgraph. For the beveled nozzle case, the width of the shear layer in the shorter lip (bottom) is slightly higher than in the longer lip. The shock cells in the jet flow field is appeared as alternate high and low velocity contour levels in the

potential core of the jet from both the circular and bevel nozzles (figure 7b and 7f). The number of shock cells present in the jet flow field looks similar for the both circular and bevel nozzle, though for the beveled nozzle case the latter shock cells are found to be weak. As expected, the width of the jet increases in the downstream locations with the introduction of secondary stream for both subsonic and supersonic cases. For the beveled primary nozzle, the secondary stream decays faster in the shorter lip side (bottom) than that in the longer lip side as seen from the velocity contours of figures 7g and 7h. *This could be due to early interaction of the secondary stream with the primary stream at the shorter lip than the longer lip.*

Contours of streamwise velocity fluctuations (u') normalized by jet exit velocity for both the cases of circular and bevel nozzle, for the subsonic and supersonic exit conditions are shown in figure 8a-h. At subsonic exit Mach number- $M_p=0.96$, both circular and bevel nozzles show the velocity fluctuations

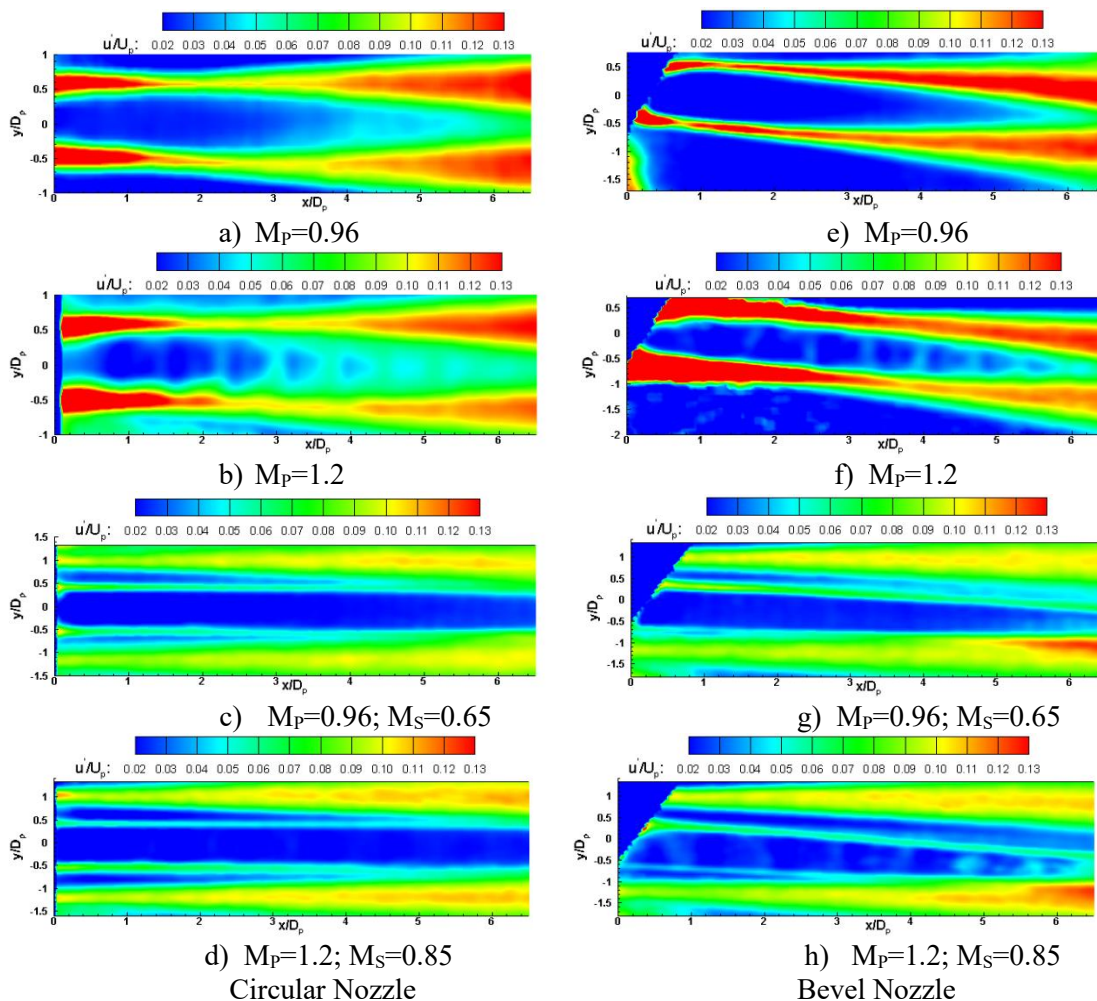


Figure 8. Mean streamwise velocity fluctuation contour of single and dual stream nozzle flow

higher in the shear layer and lower in the potential core. The bevel nozzle case shows (figure 8e) lower $u_{rms}(u')$ levels in the potential core as compared to the circular nozzle (figure 8a). The extent of the shear layer is observed to be higher in the shorter lip side of the bevel nozzle than the longer lip. The $u_{rms}(u')$ levels are higher in the shear layer at the longer lip side than that seen in the shorter lip. At $M_p=1.2$, the trend in u' levels for both the circular and beveled nozzles are similar to that seen in the subsonic case. However, u' values in the shear layer are higher than that seen in the subsonic condition (figure 8b and 8f). The increase in the u' value could be due to the presence of shock cells in the flow field. The presence of shock cells in the flow field is mildly visible in the streamwise velocity fluctuation contour as seen in figure 8b and 8f. Streamwise velocity fluctuation contour levels for the dual stream nozzle flow for the circular and bevel nozzle for $M_p=0.96$, $M_s=0.65$ is shown in figure 8c and 8g. The circular dual

stream nozzle clearly shows lower u' in the potential cores of both the primary and secondary streams (figure 8c) while higher u' is seen in the outer shear layers. The inner shear layer between the primary and the secondary streams appear to have marginally higher values of u' as compared to the values in the primary stream core.

In the dual stream flow of beveled nozzle configuration ($M_p=0.96$, $M_s=0.65$), the secondary stream

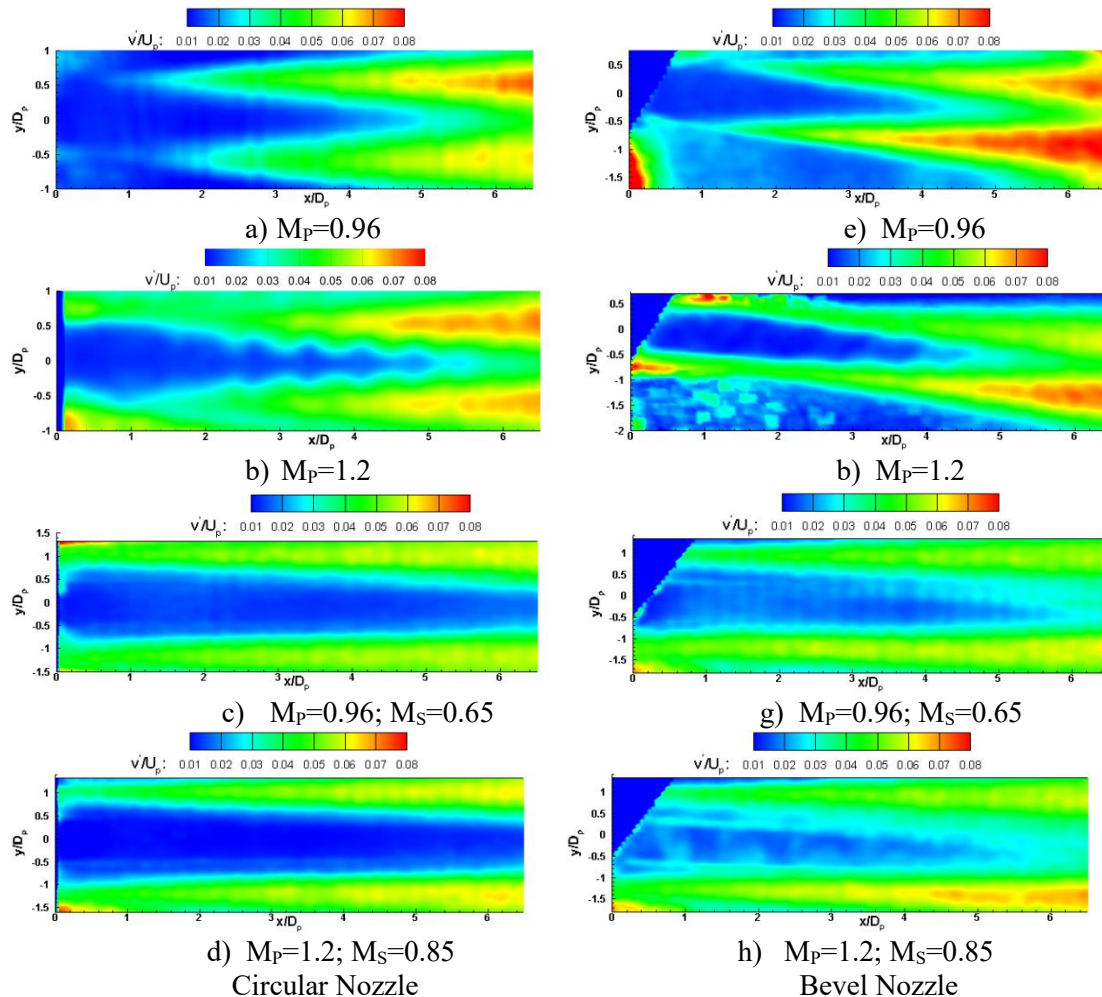


Figure 9. Mean transverse velocity fluctuation contour of single and dual stream nozzle flow

potential core is not clearly discernable at the shorter lip side as seen in the circular case wherein the streamwise velocity fluctuations (u') have lower values. However, at the longer lip side the secondary stream potential core is clearly seen since the velocity fluctuations are lower. Further, the axial extent of the low velocity fluctuation region, at the longer lip side, is larger than that seen in the circular case. The streamwise velocity fluctuation values in outer shear layer, as compared to the circular case, are lower in the longer lip side but higher in shorter lip in a small region beyond axial distance of $x/D_p=5$. At supersonic operating condition ($M_p=1.2$; $M_s=0.85$), the trend in the u' for the circular nozzle are similar to that seen in the subsonic case (figure 8c). However, the magnitude of streamwise velocity fluctuations (figure 8d) in the outer shear layer is higher than that seen in the subsonic case. In the bevel case the secondary stream potential core on the shorter lip side is seen up to an axial distance of $x/D_p=3$, while on the longer lip side it extends further (figure 8h). This is in contrast to the subsonic case where the secondary potential core on the shorter lip side is not clearly discernable (figure 8g). Weak shock patterns are visible in the primary stream potential core region similar to that seen in the mean streamwise velocity contour (figure 7).

Influence of primary nozzle exit geometry on the transverse velocity fluctuation (v') of the dual stream nozzle flow is shown in figure 9. The transverse velocity fluctuation is normalized by the primary stream jet exit velocity. Comparison of transverse velocity fluctuation contour of the primary stream from the circular and bevel nozzle at subsonic Mach number of $M_p=0.96$ is shown in figure 9a and 9e. The transverse velocity fluctuation in the shear layer is higher for the bevel nozzle compared to the circular

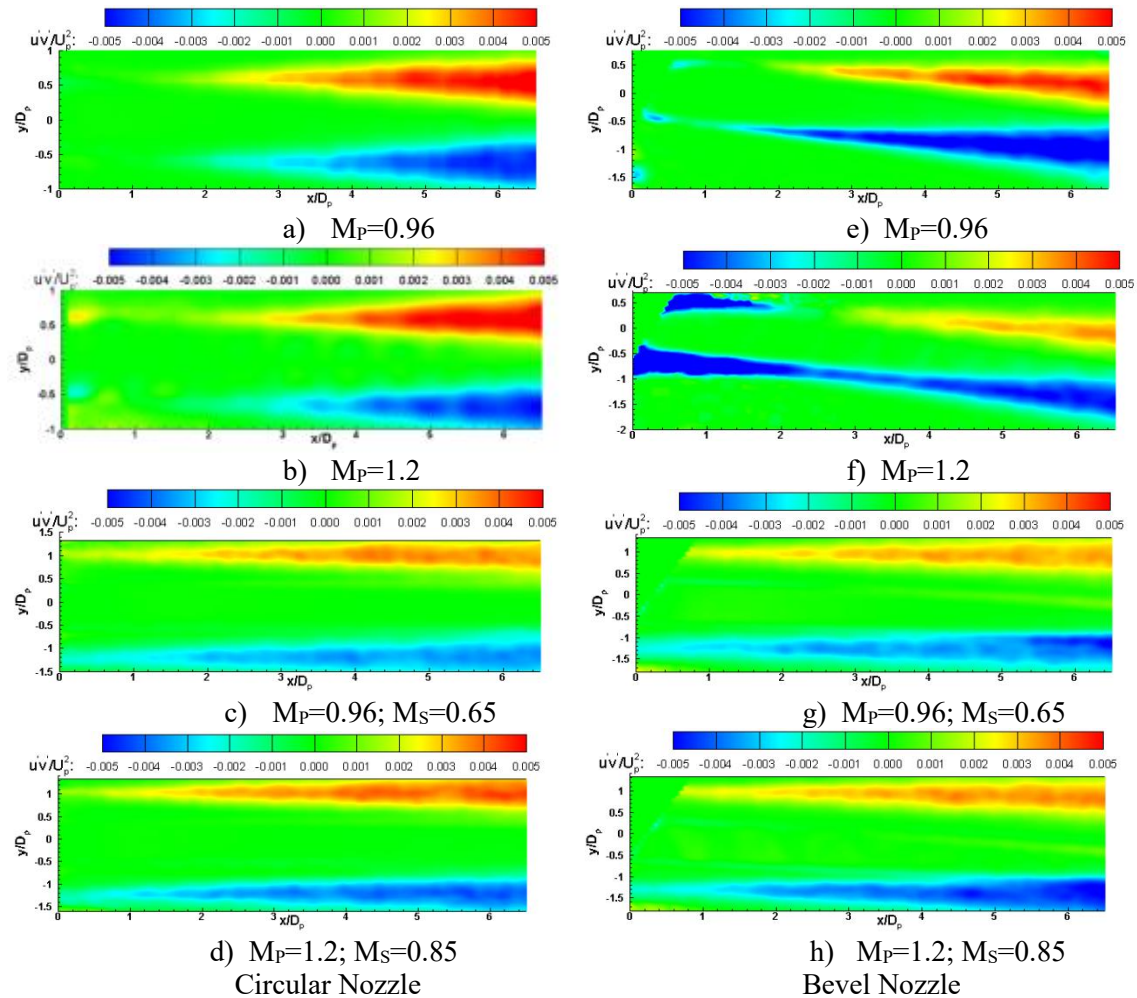


Figure 10. Mean Reynolds stress contour of single and dual stream nozzle flow

nozzle because of the transverse deflection of the flow. In the bevel nozzle case, the axial extent as well as the magnitude v' in the shear layer is higher on the shorter lip as compared to the longer lip side. At supersonic operating condition $M_p=1.2$, the trend in the transverse velocity fluctuations at the shear layer is similar to that seen in the subsonic case. A wavy pattern is seen in the v' levels at the boundary of the core of the circular and bevel nozzle jet (figure 9b) indicating the presence of shock in the jet flow field. However, the amplitude of this wavy pattern for the bevel nozzle is (figure 9f) lower than that seen in circular. Influence of secondary stream on the transverse velocity fluctuations at subsonic Mach number $M_p=0.96$; $M_s=0.65$ for the circular and bevel nozzle is shown in figure 9c and 9g. In the circular nozzle case, the axial extent of the low transverse velocity fluctuation region in the jet core is longer for dual stream case as compared to the primary stream alone case. In the bevel case, similar to the circular one the axial extent of the low fluctuation region in the potential core is increased (figure 9c) by the secondary stream. However the value is slightly higher than in the circular case. The magnitude of the v' is lower in the outer shear layer at the longer lip side as compared to the circular dual stream. Further, the fluctuations are higher in the outer shear layer at the shorter lip side than that in the longer lip side. At supersonic condition $M_p=1.2$; $M_s=0.85$, the trend of velocity fluctuation in the core and outer shear

layer is similar to that seen in the subsonic case (figure 9h). Additionally, the fluctuation values in the core and in the outer shear layer at the shorter lip are higher than dual stream flow with circular nozzle. Effect of primary nozzle exit geometry modification on the average Reynolds stress ($u'v'$) of the dual stream nozzle flow at subsonic and supersonic exit condition is shown in figure 10a-h. The Reynolds stress values are normalized by square of the jet exit velocity of the primary stream. The Reynolds stress contour for the circular nozzle shows (figure 10a and 10b) that the values in the shear layer is antisymmetric about jet axis for the primary stream alone case at Mach numbers of 0.96 and 1.2. Whereas in the bevel nozzle, the Reynolds stress has higher magnitude in the shorter lip shear layer and lower in the longer lip shear layer (figure 10e and 10f). The Reynolds stress sign change is seen in the longer lip shear layer at Mach number 1.2. Further the Reynolds stress value is higher near the exit (up to $x/D_p=2$) and lower beyond $x/D_p=2$ in both shear layers of bevel nozzle in comparison with the circular at Mach number 1.2. The Reynolds stress values are reduced significantly by the secondary stream for both circular and beveled dual stream flow. The Reynolds stress values in the outer shear layer are lower at longer lip side and higher in the shorter lip as compared to the circular nozzle for both subsonic (figure 10c and 10g) and supersonic condition (figure 10d and 10h). The values of $u'v'$ have direct influence on noise generation. Hence examination/comparison is important.

4. Conclusions

Influence of primary stream nozzle exit modification on the mean and turbulence fluctuation quantities in the near flow field of dual stream nozzle flow was experimentally investigated using 2D particle image Velocimetry. Additionally, the flow field was qualitatively visualized using shadowgraph technique. The results show that the beveling of the nozzle causes a reduction in the axial extent of shock cells compared to the circular jet, in the supersonic case. Further for the beveled nozzle case, the number of shock cells seen in the jet is less than the circular nozzle case and they are weakened by the presence of secondary stream. The flow field measurement from the 2D-PIV shows the differential shear layer growth between shorter and longer lip sides of the beveled nozzle for both supersonic and subsonic cases. The co-flowing secondary stream reduces the flow inclination angle of bevel nozzle. For the beveled nozzle case while the streamwise velocity fluctuations in the shear layer is higher at the longer lip and lower at the shorter lip, the transverse velocity fluctuation in the shear layer is lower at the longer lip and higher at the shorter lip. Introduction of secondary stream increased the potential core length due to the reduction in shear between the primary and secondary stream. The beveling of the nozzle results in Reynolds stress values being much lower for both single and dual stream configurations, when compared to the corresponding circular nozzle cases. This could be the reason for the reduction of noise level reported in the literature for the beveled nozzle.

Acknowledgments

Authors wish to acknowledge assistance of EAD Model Shop in fabricating the components of the co-flow facility.

References

- [1] Dimitri Papamoschou 2004 New method for jet noise reduction in turbofan engines *AIAA Journal* **42** 11
- [2] K. Viswanathan 2004 Parametric study of noise from dual-stream nozzles *Journal of Fluid Mechanics* **521** 35-68
- [3] Viswanathan, K 2005 Nozzle shaping for reduction of jet noise from single jets *AIAA Journal* **43** 5 1008–1022
- [4] Viswanathan, K. 2006 An elegant concept for reduction of jet noise from turbofan engines *Journal of Aircraft* **43** 3 616–626
- [5] Viswanathan, K. 2006 Noise of dual-stream beveled nozzles at supercritical pressure ratios,” *Journal of Aircraft* **43** 3 627–638
- [6] Viswanathan, K., Shur, M., Spalart, P. R., and Strelets, M. 2008 Flow and noise predictions for single and dual-stream beveled nozzles *AIAA Journal* **46** 3 601–626
- [7] K. Viswanathan, P. R. Spalart, and M. J. Czech 2011 Tailored nozzles for jet plume control and

- noise reduction *AIAA Paper* 2011-2011
- [8] Hargather, M. J., and Settles, G. S. 2009 Retroreflective shadowgraph technique for large-scale flow visualization *Applied optics* **48** 22 4449-4457